Coexistence of Quantum Hall and Quantum Anomalous Hall Phases in Disordered $MnBi_2Te_4$

Hailong Li,[1,*] Chui-Zhen Chen,[2,3,*] Hua Jiang,[2,3,†] and X. C. Xie[1,4,‡]
[1]International Center for Quantum Materials, School of Physics, Peking University, Beijing 100871, China
[2]School of Physical Science and Technology, Soochow University, Suzhou 215006, China
[3]Institute for Advanced Study, Soochow University, Suzhou 215006, China
[4]CAS Center for Excellence in Topological Quantum Computation, University of Chinese Academy of Sciences, Beijing 100190, China

(Received 12 July 2021; accepted 4 November 2021; published 3 December 2021)

In most cases, to observe quantized Hall plateaus, an external magnetic field is applied in intrinsic magnetic topological insulators $MnBi_2Te_4$. Nevertheless, whether the nonzero Chern number ($C \neq 0$) phase is a quantum anomalous Hall (QAH) state, or a quantum Hall (QH) state, or a mixing state of both is still a puzzle, especially for the recently observed $C = 2$ phase [Deng *et al.*, Science **367**, 895 (2020)]. In this Letter, we propose a physical picture based on the Anderson localization to understand the observed Hall plateaus in disordered $MnBi_2Te_4$. Rather good consistency between the experimental and numerical results confirms that the bulk states are localized in the absence of a magnetic field and a QAH edge state emerges with $C = 1$. However, under a strong magnetic field, the lowest Landau band formed with the localized bulk states, survives disorder, together with the QAH edge state, leading to a $C = 2$ phase. Eventually, we present a phase diagram of a disordered $MnBi_2Te_4$ which indicates more coexistence states of QAH and QH to be verified by future experiments.

DOI: 10.1103/PhysRevLett.127.236402

Introduction.—Since successfully synthesized in experiments [1,2], $MnBi_2Te_4$ as an intrinsic magnetic topological insulator has attracted great attention [3–10]. Intriguingly, the layered $MnBi_2Te_4$ is predicted to show plenty of exotic quantum phases, such as Weyl semimetals, quantum anomalous Hall (QAH) insulators, topological axion insulators, etc. [6,7]. However, to observe quantized Hall plateaus, it is common to apply a perpendicular magnetic field to raise the interlayer magnetic order of $MnBi_2Te_4$ [3–5]. On one hand, a magnetic field can induce an exchange gap to make it easier to observe the QAH effect [11–14], which gives rise to a higher Chern number with increasing the magnetic field [3,4]. On the other hand, the quantum Hall (QH) effect can also exist, in which case a lower Chern number corresponds to a larger magnetic field, opposite to the QAH case.

Usually, the fabricated $MnBi_2Te_4$ in experiments owns extremely low mobility from 74 to 1500 $cm^2\,V^{-1}\,s^{-1}$, indicating the presence of strong disorder [2–5]. It thus suggests that the Anderson localization [15] may have a significant influence on these systems. Nevertheless, the disorder plays quite different roles in QAH and QH effects. In QAH, the plateau transitions are mediated via disorder-induced Berry-curvature interchange [16], rather than Landau levels broadenings in the QH [17–20]. Therefore, although the disorder effect in QH and QAH effects has been both studied separately, the coexisting of them and the competing between the magnetic field and disorder in $MnBi_2Te_4$ is still promising. Previously, it has been suggested that the localized bulk states can also form Landau bands due to the magnetic-field-induced delocalization [21,22]. Such a process, especially accompanied by the coexistence of QAH and QH states, remains elusive in experiments. In this regard, the phase transitions of $MnBi_2Te_4$ under a magnetic field can be of great interest, especially for the cases with higher Chern numbers.

Recently, the observation of the QAH effect was reported in $MnBi_2Te_4$ thin flakes [3], which implies the existence of Anderson localization in a topological system. The well-developed QAH effect emerges as the Hall resistance R_{yx} reaches $-h/e^2$ under a weak magnetic field. Apart from the QAH plateau, R_{yx} goes through an additional plateau at $-h/(2e^2)$ under a strong magnetic field (see the inset of Fig. 1). The second Hall plateau is speculated as the emergence of an additional QH edge state in Ref. [3]. However, it has not been well understood because the bulk states accounting for the additional Landau band will cover the QAH edge state and lead to an unquantized Hall resistance under the weak magnetic field. Thus, it is essential to use the Anderson localization to understand the mechanism of both Hall plateaus in a unified framework, thus, help us to identify the complex phase transitions in disordered $MnBi_2Te_4$.

In this Letter, we provide a physical picture based on the Anderson localization to understand the complex phase transition from a pure QAH phase to a phase composing of QAH and QH edge states in disordered $MnBi_2Te_4$

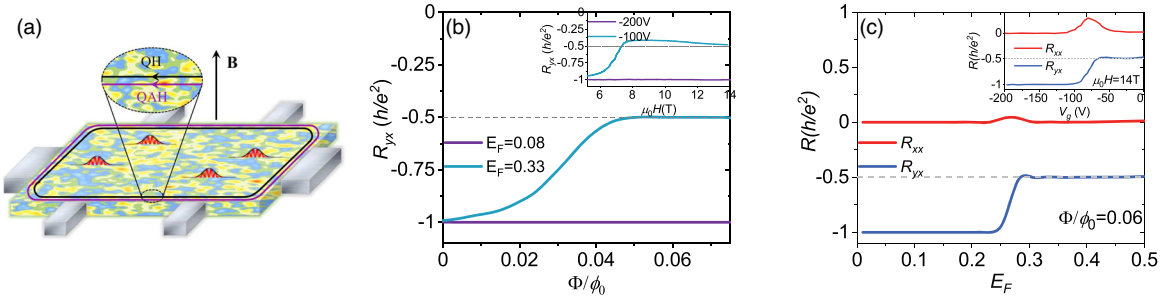

FIG. 1. (a) A schematic plot of a six-terminal disordered $MnBi_2Te_4$ device under a strong magnetic field. The wave packets represent the localized bulk states. In the absence of a magnetic field, bulk states are localized by disorder and the QAH edge state emerges. For a strong magnetic field, these localized bulk states can still form Landau bands coexisting with the QAH state. (b) Calculated Hall resistance R_{yx} as a function of magnetic field Φ/ϕ_0 under different Fermi energies. (c) Calculated longitudinal resistance R_{xx} and R_{yx} as a function of Fermi energy. The insets show the experimental measured R_{xx} and R_{yx} adopted from Ref. [3], where $\mu_0 H$ and V_g correspond to the magnetic field and Fermi energy, respectively. The numerical simulation is performed with a sample size of 400×400 sites and averaged over 320 disorder configurations.

[see Fig. 1(a)]. Via an established disordered Hamiltonian and the nonequilibrium Green's function method [23–25], we calculate the Hall resistance R_{yx} and the longitudinal resistance R_{xx} of a six-terminal device (see Fig. 1). The results are in good agreement with the experimental data. Furthermore, we capture the underlying physics by analyzing some important physical quantities, such as the localization length, the ratio of the geometric mean density of states (DOS) ρ_{typ} to the arithmetic mean DOS ρ_{ave} [26–31] and the inverse participation ratio (IPR) [30–35]. To be specific, for a high Fermi energy [see the cyan curve in Fig. 1(b)], the bulk states are localized without a magnetic field, and a $C = 1$ QAH phase emerges. However, under a strong magnetic field, localized bulk states can still form Landau bands, and the QH edge state coexists with the QAH edge state, leading to a $C = 2$ phase [see Fig. 1(b)]. Ultimately, we show a phase diagram of a disordered $MnBi_2Te_4$ which not only relates to the current experiment [3], but also indicates more coexistence states of QAH and QH waiting to be further experimentally explored.

Effective model of ferromagnetic $MnBi_2Te_4$.—Because of the confinement in the z direction of a three-dimensional (3D) $MnBi_2Te_4$ film, a two-dimensional (2D) subband model can effectively describe the underlying physics. Proceeding along the paradigm for the 3D to 2D crossover [36], the 2D effective model of a disordered ferromagnetic (FM) $MnBi_2Te_4$ takes the following form [3]

$$\mathcal{H}_{\text{eff}}^{\text{2D}} = \begin{pmatrix} h_+ & \delta \\ -\delta & h_- \end{pmatrix} + H_D, \tag{1}$$

where $h_\pm = (v_2 \pm v_4)(k_x\tau_x \pm k_y\tau_y) + [(m_0 \pm m_1) - (t_0 \pm t_1)k^2]\tau_z$ and the coupling $\delta = it_c\tau_y$. Here, v_2, v_4, m_0, t_0 are model parameters and m_1, t_1 are induced by FM order. τ_i $(i = x, y, z)$ are Pauli matrices. An external magnetic field Φ/ϕ_0 is included by doing the Peierls substitution [37] as a phase of the hopping term [38]. We consider the random disorder as $H_D = V(\mathbf{r})\tau_z$, and two parameters characterize the disorder, including the density n and strength W with $V(\mathbf{r})$ uniformly distributed within $[-W/2, W/2]$. Following the experiment [3], the model parameters for numerical calculations are fixed as $v_2 = 1.41$, $v_4 = 1.09$, $m_0 = 1.025$, $m_1 = 0.975$, $t_0 = 0.5$, $t_1 = 1.0$, $W = 4$, $n = 0.2$, and $t_c = 0.1$, unless otherwise specified.

To illustrate the physical picture clearly, we first simulate a six-terminal device based on Eq. (1) under the clean limit $W = 0$ and compare it with the experiment [3] in the Supplemental Material [39]. Evidently, the numerical results do not fit the experimental results well, especially under weak magnetic fields. However, when the disorder is involved, a detailed comparison between the numerical results and experimental data [3] shows a good agreement in Fig. 1. The following consistency between them are obtained. (1) For a high Fermi energy $E_F = 0.33$, R_{yx} starts from $-h/e^2$ as a QAH phase, transits into $-h/(2e^2)$ as a $C = 2$ Chern insulator phase [the cyan curve in Fig. 1(b)]. (2) For a lower Fermi energy $E_F = 0.08$, R_{yx} keeps $-h/e^2$ [the purple curve in Fig. 1(b)]. (3) Under a fixed magnetic field $\Phi/\phi_0 = 0.06$, R_{yx} goes from $-h/e^2$ to $-h/(2e^2)$ as R_{xx} drops to zero at the plateaus [see Fig. 1(c)]. Such a good agreement confirms that our effective model can capture the underlying physics of phase transitions in ferromagnetic $MnBi_2Te_4$ well.

Under the clean limit [40], h_+ describes a QAH insulator with a gap $m_0 + m_1$, while h_- describes a normal insulator with a smaller gap $m_0 - m_1$. In the experiment [3], the transition happening at a fixed carrier density means the additional QH state requires bulk electrons around the Fermi energy in the absence of the magnetic field. However, the observed QAH state without magnetic field and those extended bulk electrons are mutually exclusive. Thus, in the clean limit, the $C = 1$ QAH state without magnetic field and the $C = 2$ state under the magnetic field

cannot be observed simultaneously. Based on the experimental fact, the presence of disorder will make a difference. For the dirty case, the disorder tunes the extended states into localized states which is the so-called Anderson localization [15], while the QAH edge state is robust against weak disorder [41]. Consequently, the Hall resistance shows a quantized value without a magnetic field. In the presence of a magnetic field, the localized states can still collapse to form Landau bands, but disorder destroys them until the lowest Landau band survives. Then, the lowest Landau band forms a QH edge state which contributes the additional Hall plateau.

Anderson localization-induced Hall plateau.—To verify the Landau bands originates from localized bulk states in the above model, we investigate the spatial extension of the eigenstates through the ratio of the geometric mean DOS ρ_{typ} to the arithmetic mean DOS ρ_{ave} [26–31] and the inverse participation ratio (IPR) [30–35].

ρ_{ave} and ρ_{typ} are calculated in a square sample with size M under periodic boundary conditions, which are defined as [26–31]

$$\rho_{\mathrm{ave}}(E_F) = \langle\langle \rho(i, E_F) \rangle\rangle, \tag{2}$$

$$\rho_{\mathrm{typ}}(E_F) = \exp[\langle\langle \ln \rho(i, E_F) \rangle\rangle], \tag{3}$$

where $\langle\langle \cdots \rangle\rangle$ denotes the arithmetic average over the sample sites and disorder realizations. The local DOS $\rho(i, E_F)$ is calculated as $\rho(i,E_F)=\sum_{n,\alpha,\beta}|\langle i,\alpha|n,\beta\rangle|^2\delta(E_F-E_{n,\beta})$ where $|i,\alpha\rangle$ denotes an eigenstate at site i and orbital α, and n is the index for energy level. Here, we substitute $\eta/[\pi(x^2+\eta^2)]$ for $\delta(x)$ approximately with $\eta = 10^{-4}$ and use an exact diagonalization method [27]. For a extended state distributed uniformly over the sample, ρ_{typ} is almost the same as ρ_{ave}, while for a localized state concentrated on certain sites, ρ_{typ} will be extremely small. Generally, in the thermodynamic limit ($M \to \infty$), the ratio $\rho_{\mathrm{typ}}/\rho_{\mathrm{ave}}$ keeps finite for extended states, while $\rho_{\mathrm{typ}}/\rho_{\mathrm{ave}}$ approaches zero for localized states [42].

In Figs. 2(a)–2(d), we plot $\rho_{\mathrm{typ}}/\rho_{\mathrm{ave}}$ and ρ_{ave} versus Fermi energy E_F under different magnetic fields. When $\Phi/\phi_0 = 0$, in the presence of disorder, a finite ρ_{ave} in Fig. 2(c) and a small $\rho_{\mathrm{typ}}/\rho_{\mathrm{ave}}$ decreasing with size M in Fig. 2(a) indicate that the considered energy interval lies in a mobility gap rather than a bulk gap. In other words, electrons occupy the localized states. To further reveal the effect of disorder in this case, we proceed to study the average IPR defined as [30,31,34,35]

$$P^{-1} = \left\langle \frac{\sum_i |\psi_i|^4}{[\sum_i |\psi_i|^2]^2} \right\rangle \tag{4}$$

where the wave function ψ_i is evaluated at site i and E_F, and $\langle \cdots \rangle$ denotes the disorder average. As the DOS

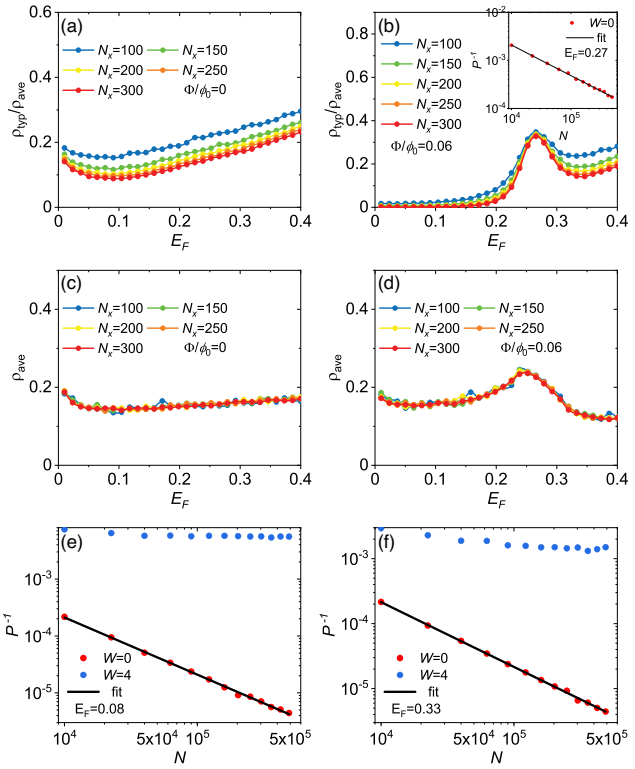

FIG. 2. (a),(b) The ratio of the geometric mean DOS ρ_{ave} to the arithmetic mean DOS ρ_{typ} with $\Phi/\phi_0 = 0$ and $\Phi/\phi_0 = 0.06$, respectively. The inset in (b) shows the IPR P^{-1} with $E_F = 0.27$. (c) and (d) show ρ_{ave} with $\Phi/\phi_0 = 0$ and $\Phi/\phi_0 = 0.06$, respectively. (e),(f) P^{-1} with $E_F = 0.08$ and $E_F = 0.33$ in the absence of magnetic field, separately. $N = M^2$ is the total sites of the sample. The blue and red points are from numerical simulation, and the black line represents a linear fit to the data. All the data are calculated with $N_x = N_y = M$.

analysis, in the thermodynamic limit ($M \to \infty$), IPR scales as $P^{-1} \propto 1/N$ with $N = M^2$ for extended states, and P^{-1} approaches constant for localized states [30,33]. In Figs. 2(e)–2(f), we investigate the effect of disorder at different E_F in the absence of magnetic field. When $W = 0$, the good linear fit of the red points shows the extended nature of the wave functions for both cases. However, when the disorder in Fig. 1 is included, the wave functions become localized which is manifested by the blue points with P^{-1} approaching constant under large sample size N. It strongly shows that disorder localizes the extended states which hide the QAH edge state in the clean limit, and leads to a quantized Hall plateau with $C = 1$ [see Fig. 1(b)]. When the external magnetic field is applied [Figs. 2(b) and 2(d)], one can identify one distinct difference from the comparison between Figs. 2(b) and 2(a) that a peak arises around $E_F = 0.27$. It refers to the lowest Landau band of which the extended states locate in its center. To prove the extended states, we calculate P^{-1} versus total sample sites N with $E_F = 0.27$. As expected, the result in the inset of Fig. 2(b) displays a linear relation in logarithmic

coordinates. On both sides of the peak, $\rho_{\mathrm{typ}}/\rho_{\mathrm{ave}}$ is small and decreases with M, which indicates two different localized phases. The two phases exactly correspond to the Hall plateaus in Fig. 1(c) and the extended states at $E_F = 0.27$ means that the $C = 2$ phase contains a QH edge state.

Localization length.—Another method to characterize the Anderson localization is to perform the finite-size scaling of localization length $\lambda(M)$. $\lambda(M)$ is calculated at Fermi energy E_F by transfer matrix method [43–47]. Generally, renormalized localization length $\Lambda(M) = \lambda/M$ increases with size M in a metallic phase, decreases with M in a localized phase, and does not depend on M at the critical point.

We consider a 2D strip of length L_y ($\sim 10^6$) and width $L_x = M$, and put the finite-size scaling result in Fig. 3. First, we focus on the lower Fermi energy $E_F = 0.08$, where $d\Lambda(M)/dM < 0$ for any magnetic field strength [see Fig. 3(a)]. According to the previous analysis, the system keeps $C = 1$ as a QAH phase with a varying magnetic field. However, for $E_F = 0.33$, two critical points arise [see Fig. 3(b)]. With an increase in the magnetic field, the system starts from a QAH insulator with $C = 1$, undergoes a phase transition, and arrives at a Chern insulator with $C = 2$ which is the phase in Fig. 2(b). Thus, such a $C = 2$ phase is a coexistence state of QH and QAH phases. This is consistent with the six-terminal Hall calculation in Fig. 1(b). For stronger magnetic fields, the system will come back to a QAH insulator with $C = 1$ due to the shift of Landau bands.

Next, we turn to focus on $\Lambda(M)$ versus E_F with fixed magnetic field [see Figs. 3(c) and 3(d)]. When $\Phi/\phi_0 = 0.06$, the result in Fig. 3(c) shows the distribution of Landau bands, and the peaks account for the extended states in their center. In such a case, the lower Landau bands are more robust against disorder, whereas the higher Landau bands are so weak that $\Lambda(M)$ collapses together and peaks disappear gradually. For a larger magnetic field, e.g., $\Phi/\phi_0 = 0.09$ in Fig. 3(d), each Landau band moves to higher energy, and more Landau bands become stable which can contribute more Hall plateaus.

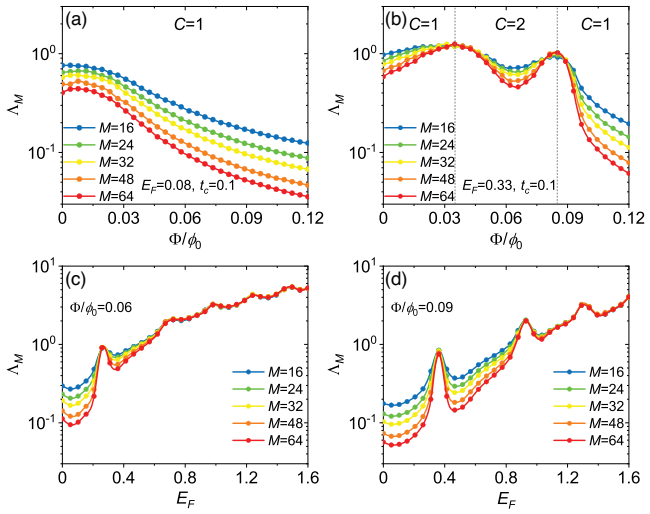

FIG. 3. (a),(b) Renormalized localization length $\Lambda_M = \lambda(M)/M$ against the magnetic field Φ/ϕ_0 with different Fermi energies. (c),(d) Λ_M as a function of Fermi energy under different magnetic field strengths. The calculation is performed with the periodic boundary condition in the x direction.

Phase diagram and discussions.—To illustrate the physical picture completely, we calculate the localization length versus Fermi energy under different magnetic fields and summarize a phase diagram in Fig. 4. Specifically, at small magnetic fields or low Fermi energies, the system is in a QAH phase with $C = 1$ (the pink region in Fig. 4), while for large magnetic fields or high Fermi energies, the system is in a coexistence phase of QH and QAH with $C \geq 2$ (the blue region in Fig. 4) and the solid line indicates the phase boundary [19,20,48–51]. For example, $E_F = 0.33$ or $\Phi/\phi_0 = 0.06$ corresponds to the scenario observed in experiment [3]. It is also remarkable to note that for a much higher Fermi energy in the phase diagram, such as $E_F = 0.8$, the system will start from a $C = 1$ QAH phase and go through a $C = 3$ phase before arriving at the $C = 2$ phase. An evident dip of Hall resistance R_{yx} toward $h/(3e^2)$ between h/e^2 and $h/(2e^2)$ in experiment [3] implies the existence of such a $C = 3$ phase. Thus, the phase diagram predicts more coexistence states of QAH and QH effect with higher Chern numbers to be verified by further experiments. To observe the higher Chern numbers, it is required to improve the quality of samples, i.e., cleaner samples, which will make it easier to realize Landau quantization under smaller magnetic fields. Moreover, for a thicker sample which may show $C = 2$ QAH phase [4], the coexisting state can even comprise a $C = 2$ QAH state and a $C \neq 0$ QH state under the magnetic field. Another possible coexisting phase with counterpropagating

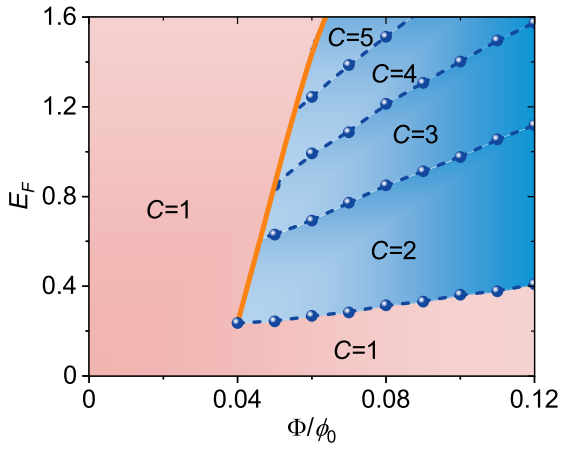

FIG. 4. Phase diagram of a disordered ferromagnetic insulator $MnBi_2Te_4$ in the $E_F - \Phi/\phi_0$ plane. The blue balls mark the extended states of Landau bands. The phase diagram is identified from the renormalized localization length Λ_M.

QAH ($C = 1$) and QH ($C = -1$) edge states was proposed in the clean HgTe/CdTe quantum well [52]. Furthermore, in experiments, the participation of QH edge states in a QAH system can be distinguished by examining the variation of quantized Hall resistance under different magnetic fields.

Conclusion.—To summarize, we investigate a disordered $MnBi_2Te_4$ under an external magnetic field and find that the exotic Hall plateaus in the experiment [3] originate from physics of the Anderson localization. In the absence of a magnetic field, disorder localizes the bulk states within the QAH bulk energy gap and gives rise to a $C = 1$ phase. However, under an external magnetic field, the lowest Landau band, formed by those localized states, survives disorder and together with the QAH edge state, they lead to a $C = 2$ phase. Our work can help to distinguish the complex phase transitions of disordered $MnBi_2Te_4$ in the presence of a magnetic field, and also stimulates further experiments to observe more coexistence states of QAH and QH.

We thank Yuanbo Zhang for illuminating discussions. This work is financially supported by the National Basic Research Program of China (Grants No. 2019YFA0308403 and No. 2015CB921102), the National Natural Science Foundation of China (Grants No. 11974256, and No. 11822407), and the Strategic Priority Research Program of the Chinese Academy of Sciences (Grant No. XDB28000000). C.-Z. C. is also funded by the Natural Science Foundation of Jiangsu Province Grant No. BK20190813 and the Priority Academic Program Development (PAPD) of Jiangsu Higher Education Institutions.

Note added.—Recently, we became aware of an independent experimental study [53] of which the observed phase diagram is consistent with our predictions.

*These authors contributed equally to this work.
†jianghuaphy@suda.edu.cn
‡xcxie@pku.edu.cn

[1] M. M. Otrokov, T. V. Menshchikova, M. G. Vergniory, I. P. Rusinov, A. Yu Vyazovskaya, Y. M. Koroteev, G. Bihlmayer, A. Ernst, P. M. Echenique, A. Arnau, and E. V. Chulkov, Highly-ordered wide bandgap materials for quantized anomalous hall and magnetoelectric effects, 2D Mater. **4**, 025082 (2017).
[2] Y. Gong *et al.*, Experimental realization of an intrinsic magnetic topological insulator, Chin. Phys. Lett. **36**, 076801 (2019).
[3] Y. Deng, Y. Yu, M. Z. Shi, Z. Guo, Z. Xu, J. Wang, X. H. Chen, and Y. Zhang, Quantum anomalous Hall effect in intrinsic magnetic topological insulator $MnBi_2Te_4$, Science **367**, 895 (2020).
[4] J. Ge, Y. Liu, J. Li, H. Li, T. Luo, Y. Wu, Y. Xu, and J. Wang, High-Chern-number and high-temperature quantum Hall effect without Landau levels, Natl. Sci. Rev. **7**, 1280 (2020).
[5] C. Liu, Y. Wang, H. Li, Y. Wu, Y. Li, J. Li, K. He, Y. Xu, J. Zhang, and Y. Wang, Robust axion insulator and Chern insulator phases in a two-dimensional antiferromagnetic topological insulator, Nat. Mater. **19**, 522 (2020).
[6] D. Zhang, M. Shi, T. Zhu, D. Xing, H. Zhang, and J. Wang, Topological Axion States in the Magnetic Insulator $MnBi_2Te_4$ with the Quantized Magnetoelectric Effect, Phys. Rev. Lett. **122**, 206401 (2019).
[7] J. Li, Y. Li, S. Du, Z. Wang, B.-L. Gu, S.-C. Zhang, K. He, W. Duan, and Y. Xu, Intrinsic magnetic topological insulators in van der Waals layered $MnBi_2Te_4$-family materials, Sci. Adv. **5**, eaaw5685 (2019).
[8] M. M. Otrokov *et al.*, Prediction and observation of an antiferromagnetic topological insulator, Nature (London) **576**, 416 (2019).
[9] R.-X. Zhang, F. Wu, and S. Das Sarma, Möbius Insulator and Higher-Order Topology in $MnBi_{2n}Te_{3n+1}$, Phys. Rev. Lett. **124**, 136407 (2020).
[10] Y.-J. Hao *et al.*, Gapless Surface Dirac Cone in Antiferromagnetic Topological Insulator $MnBi_2Te_4$, Phys. Rev. X **9**, 041038 (2019).
[11] C.-X. Liu, X.-L. Qi, X. Dai, Z. Fang, and S.-C. Zhang, Quantum Anomalous Hall Effect in $Hg_{1-y}Mn_yTe$ Quantum Wells, Phys. Rev. Lett. **101**, 146802 (2008).
[12] R. Yu, W. Zhang, H.-J. Zhang, S.-C. Zhang, X. Dai, and Z. Fang, Quantized anomalous Hall effect in magnetic topological insulators, Science **329**, 61 (2010).
[13] C.-Z. Chang *et al.*, Experimental observation of the quantum anomalous Hall effect in a magnetic topological insulator, Science **340**, 167 (2013).
[14] C.-X. Liu, S.-C. Zhang, and X.-L. Qi, The quantum anomalous Hall effect: Theory and experiment, Annu. Rev. Condens. Matter Phys. **7**, 301 (2016).
[15] P. W. Anderson, Absence of diffusion in certain random lattices, Phys. Rev. **109**, 1492 (1958).
[16] Z. Qiao, Y. Han, L. Zhang, K. Wang, X. Deng, H. Jiang, S. A. Yang, J. Wang, and Q. Niu, Anderson Localization from the Berry-Curvature Interchange in Quantum Anomalous Hall Systems, Phys. Rev. Lett. **117**, 056802 (2016).
[17] S. Kivelson, D.-H. Lee, and S.-C. Zhang, Global phase diagram in the quantum Hall effect, Phys. Rev. B **46**, 2223 (1992).
[18] A. W. W. Ludwig, M. P. A. Fisher, R. Shankar, and G. Grinstein, Integer quantum Hall transition: An alternative approach and exact results, Phys. Rev. B **50**, 7526 (1994).
[19] D. Z. Liu, X. C. Xie, and Q. Niu, Weak Field Phase Diagram for an Integer Quantum Hall Liquid, Phys. Rev. Lett. **76**, 975 (1996).
[20] D. N. Sheng and Z. Y. Weng, Disappearance of Integer Quantum Hall Effect, Phys. Rev. Lett. **78**, 318 (1997).
[21] T. Ando, Numerical study of symmetry effects on localization in two dimensions, Phys. Rev. B **40**, 5325 (1989).
[22] M. Y. Azbel', Quantum particle in a random potential: Exact solution and its implications, Phys. Rev. B **45**, 4208 (1992).
[23] A. MacKinnon, The calculation of transport properties and density of states of disordered solids, Z. Phys. B **59**, 385 (1985).

[24] A.-P. Jauho, N. S. Wingreen, and Y. Meir, Time-dependent transport in interacting and noninteracting resonant-tunneling systems, Phys. Rev. B **50**, 5528 (1994).
[25] K. Y. Camsari, S. Chowdhury, and S. Datta, The non-equilibrium green function (NEGF) method, arXiv:2008.01275.
[26] Y.-Y. Zhang, R.-L. Chu, F.-C. Zhang, and S.-Q. Shen, Localization and mobility gap in the topological anderson insulator, Phys. Rev. B **85**, 035107 (2012).
[27] Y.-Y. Zhang and S.-Q. Shen, Algebraic and geometric mean density of states in topological anderson insulators, Phys. Rev. B **88**, 195145 (2013).
[28] V. Dobrosavljević, A. A. Pastor, and B. K. Nikolić, Typical medium theory of Anderson localization: A local order parameter approach to strong-disorder effects, Europhys. Lett. **62**, 76 (2003).
[29] G. Schubert, J. Schleede, K. Byczuk, H. Fehske, and D. Vollhardt, Distribution of the local density of states as a criterion for Anderson localization: Numerically exact results for various lattices in two and three dimensions, Phys. Rev. B **81**, 155106 (2010).
[30] M. Janssen, Statistics and scaling in disordered mesoscopic electron systems, Phys. Rep. **295**, 1 (1998).
[31] J. H. Pixley, P. Goswami, and S. Das Sarma, Anderson Localization and the Quantum Phase Diagram of Three Dimensional Disordered Dirac Semimetals, Phys. Rev. Lett. **115**, 076601 (2015).
[32] R. J. Bell and P. Dean, Atomic vibrations in vitreous silica, Discuss. Faraday Soc. **50**, 55 (1970).
[33] J. T. Edwards and D. J. Thouless, Numerical studies of localization in disordered systems, J. Phy. C **5**, 807 (1972).
[34] F. Wegner, Inverse participation ratio in $2+\epsilon$ dimensions, Z. Phys. B **36**, 209 (1980).
[35] Y.-Y. Zhang, J. Hu, B. A. Bernevig, X. R. Wang, X. C. Xie, and W. M. Liu, Localization and the Kosterlitz-Thouless Transition in Disordered Graphene, Phys. Rev. Lett. **102**, 106401 (2009).
[36] X.-L. Qi and S.-C. Zhang, Topological insulators and superconductors, Rev. Mod. Phys. **83**, 1057 (2011).
[37] D. R. Hofstadter, Energy levels and wave functions of Bloch electrons in rational and irrational magnetic fields, Phys. Rev. B **14**, 2239 (1976).
[38] The strength Φ/ϕ_0 is the magnetic flux through a unit cell in units of the flux quantum.
[39] See Supplemental Material at http://link.aps.org/supplemental/10.1103/PhysRevLett.127.236402 for detailed discussions.
[40] h_+ decouples with h_- when $t_c = 0$, which is helpful for theoretical analysis. However, a small coupling δ will not change the results qualitatively.
[41] C.-X. Liu, S.-C. Zhang, and X.-L. Qi, The quantum anomalous Hall effect: Theory and experiment, Annu. Rev. Condens. Matter Phys. **7**, 301 (2016).
[42] A. Weiße, G. Wellein, A. Alvermann, and H. Fehske, The kernel polynomial method, Rev. Mod. Phys. **78**, 275 (2006).
[43] A. MacKinnon and B. Kramer, One-Parameter Scaling of Localization Length and Conductance in Disordered Systems, Phys. Rev. Lett. **47**, 1546 (1981).
[44] A. MacKinnon and B. Kramer, The scaling theory of electrons in disordered solids: Additional numerical results, Z. Phys. B **53**, 1 (1983).
[45] B. Kramer and A. MacKinnon, Localization: Theory and experiment, Rep. Prog. Phys. **56**, 1469 (1993).
[46] K. Slevin and T. Ohtsuki, Critical exponent for the Anderson transition in the three-dimensional orthogonal universality class, New J. Phys. **16**, 015012 (2014).
[47] Z.-Q. Zhang, C.-Z. Chen, Y. Wu, H. Jiang, J. Liu, Q.-f. Sun, and X. C. Xie, Chiral interface states and related quantized transport in disordered Chern insulators, Phys. Rev. B **103**, 075434 (2021).
[48] H. W. Jiang, C. E. Johnson, K. L. Wang, and S. T. Hannahs, Observation of Magnetic-Field-Induced Delocalization: Transition from Anderson Insulator to Quantum Hall Conductor, Phys. Rev. Lett. **71**, 1439 (1993).
[49] C.-T. Liang, L.-H. Lin, C. Kuang Yoa, S.-T. Lo, Y.-T. Wang, D.-S. Lou, G.-H. Kim, C. Yuan-Huei, Y. Ochiai, N. Aoki, J.-C. Chen, Y. Lin, H. Chun-Feng, S.-D. Lin, and D. A. Ritchie, On the direct insulator-quantum Hall transition in two-dimensional electron systems in the vicinity of nano-scaled scatterers, Nanoscale Res. Lett. **6**, 131 (2011).
[50] A. P. Savelyev, S. V. Gudina, Y. G. Arapov, V. N. Neverov, S. M. Podgonykh, and M. V. Yakunin, Insulator-quantum Hall transition in n-InGaAs/GaAs heterostructures, Low Temp. Phys. **43**, 491 (2017).
[51] T. Wang, K. P. Clark, G. F. Spencer, A. M. Mack, and W. P. Kirk, Magnetic-Field-Induced Metal-Insulator Transition in Two Dimensions, Phys. Rev. Lett. **72**, 709 (1994).
[52] J. Böttcher, C. Tutschku, L. W. Molenkamp, and E. M. Hankiewicz, Survival of the Quantum Anomalous Hall Effect in Orbital Magnetic Fields as a Consequence of the Parity Anomaly, Phys. Rev. Lett. **123**, 226602 (2019).
[53] J. Cai, D. Ovchinnikov, Z. Fei, M. He, T. Song, Z. Lin, C. Wang, D. Cobden, J.-H. Chu, Y.-T. Cui *et al.*, Electric control of a canted-antiferromagnetic Chern insulator, arXiv:2107.04626.